J. Fluid Mech. (1994), *vol.* 264, *pp.* 255–275

Transient and asymptotic stability of granular shear flow

By P. J. SCHMID[1]† AND H. K. KYTÖMAA[2]

[1] Department of Mathematics, Massachusetts Institute of Technology, Cambridge, MA 02139, USA

[2] Department of Mechanical Engineering, Massachusetts Institute of Technology, Cambridge, MA 02139, USA

(Received 30 December 1992 and in revised form 17 September 1993)

The linear stability of granular material in an unbounded uniform shear flow is considered. Linearized equations of motion derived from kinetic theories are used to arrive at a linear initial-value problem for the perturbation quantities. Two cases are investigated: (*a*) wavelike disturbances with time constant wavenumber vector, and (*b*) disturbances that will change their wave structure in time owing to a shear-induced tilting of the wavenumber vector. In both cases, the stability analysis is based on the solution operator whose norm represents the maximum possible amplification of initial perturbations. Significant transient growth is observed which has its origin in the non-normality of the involved linear operator. For case (*a*), regions of asymptotic instability are found in the two-dimensional wavenumber plane, whereas case (*b*) is found to be asymptotically stable for all physically meaningful parameter combinations. Transient linear stability phenomena may provide a viable and fast mechanism to trigger finite-amplitude effects, and therefore constitute an important part of pattern formation in rapid particulate flows.

1. Introduction

Rapid flows of granular materials arise in numerous applications in science and engineering. In materials processing, ceramic powders are chemically precipitated out of gas phase reactions in turbulent flows, in power generation circulating fluidized bed combustors are used to burn coal, in chemical processing pneumatic transport is widely used in a variety of situations, and in the environment, sediment is transported along river beds or on the ocean floor, and debris, soil and rocks flow down steep hill sides leaving trails of destruction.

Despite a great deal of effort directed towards modelling the constitutive equations beyond the ground breaking work of Bagnold (1954) (Jenkins & Savage 1983; Savage 1992), and simulating particulate systems with direct numerical approaches by computing all interactions separately (e.g. Walton, Kim & Rosato 1991; see review by Campbell 1990), our understanding of inertially dominated granular flow phenomena still lacks a satisfactory theoretical background. The principal deficiency lies in the fact that most of the above examples are affected by fluid–particle interactions in a turbulent flow field with a solids loading that cannot be assumed to be small, and as a consequence we have difficulty predicting the highly non-uniform particulate distributions that have been observed in these applications.

† Current address: Department of Applied Mathematics, FS-20, University of Washington, Seattle, WA 98195, USA.

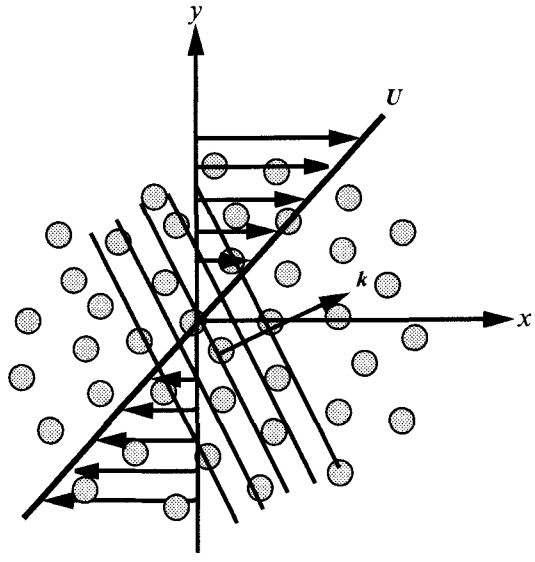

FIGURE 1. Schematic of the flow geometry. Shown is the constant shear mean velocity profile $U(y)$, the orientation of the coordinate axes x and y and the superimposed wavelike disturbance of infinitesimal amplitude and wave vector $\boldsymbol{k}$.

However, coherent granular features have been observed in flow simulations free of fluid effects (Hopkins & Louge 1991), and their appearance may be attributed to a selection principle based on the stability of organized structures. Until the work of Savage (1992) which makes effective use of symbolic manipulation, little attention had been paid to the stability issues of granular flows. Savage (1992) used equations of motion derived by Lun *et al.* (1984) from kinetic theory and analysed the stability of the linearized system using eigenvalue techniques. The same approach was used by Babić (1992, 1993) to demonstrate that if a granular system is sufficiently small, it will always be stable as the unstable low wavenumber cannot exist. A similar approach has been used by many in the context of two-fluid models to study the formation and propagation of concentration inhomogeneities (Anderson & Jackson 1968; Hill & Bedford 1979; Jackson 1985; Prosperetti & Jones 1987; Batchelor 1988; Homsy, El-Kaissy & Didwania 1980; Foscolo & Gibilaro 1987). More recently McNamara (1993) has considered the stability of granular systems in the dense limit using equations due to Haff (1983). This work describes the sound and heat conduction modes as does the work of Mello, Diamond & Levine (1991) with a lesser constraint on solid fraction.

Inertially dominated granular flows as well as non-zero Reynolds number fluidization are inherently nonlinear. If initial perturbations grow sufficiently large, nonlinear effects will become important. To predict the onset of such finite-amplitude effects, it is essential to investigate the transient character of the linear problem, and the eigenvalue approach cannot provide this insight for the case of a non-normal linear evolution operator. In the context of viscous Newtonian flows, it has been shown (Butler & Farrell 1992; Reddy, Schmid & Henningson 1993; Reddy & Henningson 1993; Trefethen *et al.* 1993; Farrell & Ioannou 1993) that the linear evolution operator supports solutions that will transiently amplify the initial perturbation energy by orders of magnitude although all of the eigenvalues are confined to the stable half-plane.

The present paper addresses the linear stability of pure shear flows of dry particles

that interact by colliding nearly elastically against one another to determine whether transient effects may lead to sufficient growth that may then render the linear system invalid. The analysis is based on the linearized equations due to Lun *et al.* (1984) for the evolution of infinitesimal perturbations. Our stability analysis will follow a different route that will enable us to capture transient as well as long-time phenomena. The analysis will rest upon the norm of the matrix exponential or the fundamental matrix rather than on eigenvalues, and its relation to eigenvalue-based stability analysis will be established and critically assessed.

2. Governing equations

We will investigate the flow of a mixture consisting of rigid smooth particles embedded in an incompressible and inviscid fluid of infinite extent. A linear velocity profile is assumed,

$$\boldsymbol{U}(y) = \Gamma y \boldsymbol{e}_x,$$

where Γ is the (constant) shear rate and $\boldsymbol{e}_x$ is the unit vector in the streamwise direction. For a sketch of the flow geometry see figure 1.

The governing equations for the conservation of mass, momentum and energy are written as follows:

$$\frac{\mathrm{d}\nu}{\mathrm{d}t} = -\nu \nabla \boldsymbol{u},$$

$$\nu \frac{\mathrm{d}\boldsymbol{u}}{\mathrm{d}t} = \nu \boldsymbol{g} - \nabla \boldsymbol{p},$$

$$\tfrac{3}{2}\nu \frac{\mathrm{d}T}{\mathrm{d}t} = -\boldsymbol{p} : \nabla \boldsymbol{u} - \nabla \boldsymbol{q} - \gamma,$$

where ν denotes the solid fraction, $\boldsymbol{u}$ is the bulk velocity, $\boldsymbol{p}$ is the stress tensor, $\boldsymbol{g}$ is the acceleration due to gravity and T denotes the granular temperature; $\boldsymbol{q}$ stands for the flux of fluctuation energy and γ is the collisional rate of energy dissipation per unit volume.

The equations above have been non-dimensionalized by the diameter of the solid particles and the shear rate Γ. We will restrict ourselves to the case of two-dimensional disturbances. To close the above equations we make use of the constitutive equations derived by Lun *et al.* (1984) and further simplify them by keeping only first-order terms in the small parameter $(1-e)$ where e denotes the coefficient of restitution, thereby restricting our attention to systems that exhibit nearly elastic collisions. After linearizing about a steady state (which we will denote with the subscript 0) we arrive at the evolution equations for the disturbance quantities.

Next, we express the perturbation quantities (denoted by a prime) in the form

$$\begin{pmatrix} \nu' \\ u' \\ v' \\ T' \end{pmatrix} = \begin{pmatrix} \hat{\nu} \\ \hat{u} \\ \hat{v} \\ \hat{T} \end{pmatrix} \exp\left[\mathrm{i}\boldsymbol{k}^T(t)\,\boldsymbol{x}\right],$$

with $$\boldsymbol{x} = [x \quad y]^T, \qquad \boldsymbol{k}^T(t) = [k_x(t) \quad k_y(t)].$$

Notice that the streamwise and normal wavenumber, k_x and k_y respectively, have been assumed to vary in time. Following Phillips (1969), we will consider a simple

model that will mimic the interaction of the disturbances with the mean flow. This model has the form of Fourier modes in which the wavenumber vector $\boldsymbol{k}$ is turned by the mean shear flow.

$$\boldsymbol{k}(t) = [k_x(0), \quad k_y(0) - tk_x(0)].$$

Whereas the x-component of $\boldsymbol{k}$ remains constant, the y-component will vary linearly in time leading to phase lines nearly parallel to the x-axis as time progresses. Figure 2 shows a sketch of the wavelike structures for both positive and negative normal wavenumber k_y.

Substituting the above assumptions and simplifications into the governing equations leads to the equations governing the evolution of the wave amplitudes of an infinitesimal perturbation about a steady mean state

$$\frac{\mathrm{d}\hat{v}}{\mathrm{d}t} = -\mathrm{i}\nu_0(k_x\hat{u} + k_y\hat{v}),$$

$$\frac{\mathrm{d}\hat{u}}{\mathrm{d}t} = -\frac{\mathrm{i}}{\nu_0}\left[T_0\frac{\partial F_1}{\partial \nu}\bigg|_o k_x - \frac{1}{2}\frac{\partial F_2}{\partial \nu}\bigg|_o k_y\right]\hat{v} - \frac{1}{\nu_0}[(\alpha_0 + \tfrac{2}{3}F_2|_o)k_x^2 + \tfrac{1}{2}F_2|_o k_y^2]\hat{u}$$

$$-\frac{1}{\nu_0}[(\alpha_0 + \tfrac{1}{6}F_2|_o)k_x k_y + \nu_0]\hat{v} - \frac{\mathrm{i}}{\nu_0}\left[F_1|_o k_x - \frac{1}{2}\frac{\partial F_2}{\partial T}\bigg|_o k_y\right]\hat{T},$$

$$\frac{\mathrm{d}\hat{v}}{\mathrm{d}t} = -\frac{\mathrm{i}}{\nu_0}\left[T_0\frac{\partial F_1}{\partial \nu}\bigg|_o k_y - \frac{1}{2}\frac{\partial F_2}{\partial \nu}\bigg|_o k_x\right]\hat{v} - \frac{1}{\nu_0}[(\alpha_0 + \tfrac{1}{6}F_2|_o)k_x k_y]\hat{u}$$

$$-\frac{1}{\nu_0}[(\alpha_0 + \tfrac{2}{3}F_2|_o)k_y^2 + \tfrac{1}{2}F_2|_o k_x^2]\hat{v} - \frac{\mathrm{i}}{\nu_0}\left[F_1|_o k_y - \frac{1}{2}\frac{\partial F_2}{\partial T}\bigg|_o k_x\right]\hat{T},$$

$$\frac{\mathrm{d}\hat{T}}{\mathrm{d}t} = -\frac{2}{3\nu_0}\left[\frac{\partial \gamma}{\partial \nu}\bigg|_o - \frac{1}{2}\frac{\partial F_2}{\partial \nu}\bigg|_o\right]\hat{v} - \frac{2\mathrm{i}}{3\nu_0}[\bar{p}_0 k_x - F_2|_o k_y]\hat{u}$$

$$-\frac{2\mathrm{i}}{3\nu_0}[\bar{p}_0 k_y - F_2|_o k_x]\hat{v} - \frac{2}{3\nu_0}\left[-\frac{1}{2}\frac{\partial F_2}{\partial T}\bigg|_o + \frac{\partial \gamma}{\partial T}\bigg|_o + K_0(k_x^2 + k_y^2)\right]\hat{T},$$

with

$$F_1 = \nu(1 + 4\nu g_0),$$

$$\alpha = \tfrac{8}{3}\nu^2 g_0\left(\frac{T}{\pi}\right)^{\frac{1}{2}},$$

$$F_2 = \frac{5\pi}{48 g_0}(1 + \tfrac{8}{5}\nu g_0)^2\left(\frac{T}{\pi}\right)^{\frac{1}{2}} + \tfrac{16}{5}\nu^2 g_0\left(\frac{T}{\pi}\right)^{\frac{1}{2}} = F_3\left(\frac{T}{\pi}\right)^{\frac{1}{2}},$$

$$K = \frac{1}{g_0}\left[\frac{25\pi}{128}(1 + \tfrac{12}{5}\nu g_0)^2 + 4(\nu g_0)^2\right]\left(\frac{T}{\pi}\right)^{\frac{1}{2}},$$

$$\gamma = \frac{24}{\pi^{\frac{1}{2}}}(1 - e)\,\nu^2 g_0\, T^{\frac{3}{2}},$$

$$g_0 = \frac{2 - \nu}{2(1 - \nu)^3}.$$

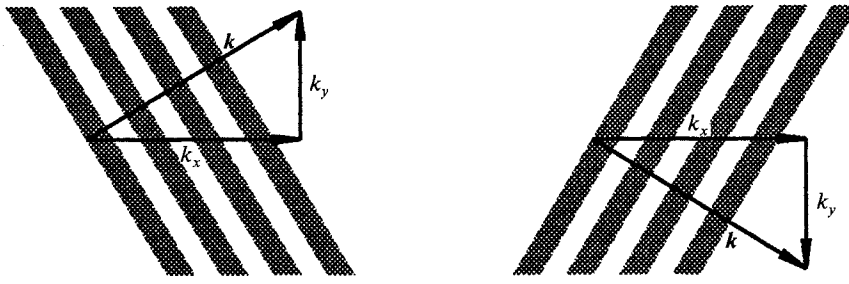

FIGURE 2. Sketch of wavelike pattern for (*a*) both the streamwise and normal wavenumber positive, (*b*) the streamwise wavenumber positive, the normal wavenumber negative.

These equations are taken from Savage (1992) and have been reproduced for completeness. For a derivation of these equations the reader is referred to the original reference.

The above equations constitute a system of differential equations with variable coefficients and read

$$\frac{\mathrm{d}}{\mathrm{d}t}\boldsymbol{q} = \boldsymbol{A}(t)\,\boldsymbol{q} \quad \text{with} \quad \boldsymbol{q} = (\hat{v}\,\hat{u}\,\hat{v}\,\hat{T})^T. \tag{1}$$

For the model of shear-induced wave vector turning proposed above, $\boldsymbol{A}(t)$ is quadratic in time and can be written as

$$\boldsymbol{A}(t) = \boldsymbol{A}_0 + \boldsymbol{A}_1 t + \boldsymbol{A}_2 t^2$$

with time-constant matrices $\boldsymbol{A}_0, \boldsymbol{A}_1$ and $\boldsymbol{A}_2$.

3. Stability analysis

In this section we will focus on two different cases of equation (1). The case of time-independent wave vectors will be treated first and a stability calculus based on the norm of the matrix exponential will be introduced to probe the stability characteristics of the flow variables. The derived tools will then be extended to the case of time-dependent wavenumbers where the special case of shear-induced wave vector turning will be considered. Both cases will lead to similar stability criteria, although the mathematical structure will be markedly different.

3.1. *Constant wave vector case* $\boldsymbol{A}(t) = \boldsymbol{A}_0$

The formal solution of the governing equation (1) for constant $\boldsymbol{A}$ can be expressed in the form

$$\boldsymbol{q} = \exp(t\boldsymbol{A})\,\boldsymbol{q}_0 = \boldsymbol{S}\exp(t\Lambda)\,\boldsymbol{S}^{-1}\boldsymbol{q}_0,$$

where Λ stands for the diagonal matrix with the eigenvalues of $\boldsymbol{A}$ along its diagonal and $\boldsymbol{S}$ denotes the matrix whose columns are composed of the normalized eigenvectors of $\boldsymbol{A}$.

A widespread method in linear stability analysis is to concentrate on $\exp(t\Lambda)$, i.e. the spectrum of $\boldsymbol{A}$ in order to analyse the behaviour of $\boldsymbol{q}$. This is only justified when the matrix $\boldsymbol{A}$ is of normal type because only in this case do the eigenvectors form an orthogonal set that results in a unitary $\boldsymbol{S}$. If the matrix $\boldsymbol{A}$ is non-normal (as in our case), basing stability solely on $\exp(t\Lambda)$ can be misleading, as owing to the similarity transform based on a non-unitary matrix $\boldsymbol{S}$, transient phenomena may occur which are not captured by the spectrum alone.

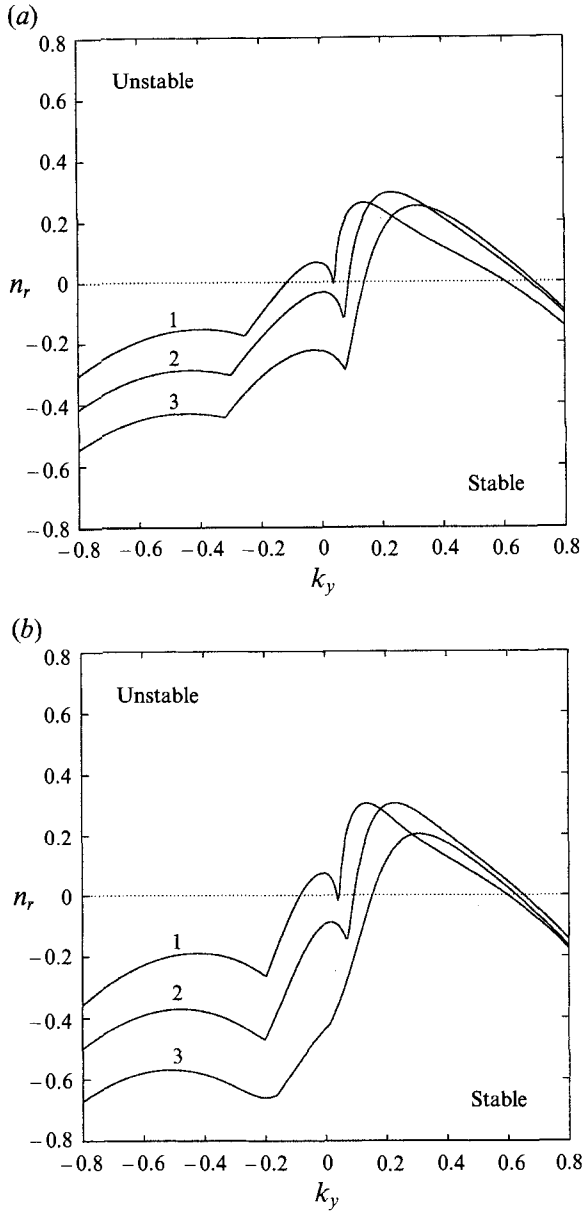

FIGURE 3. Asymptotic growth rate n_r versus normal wavenumber k_y. The curves labelled with 1, 2 and 3 correspond to a streamwise wavenumber $k_x = 0.1$, 0.2, 0.3, respectively. (*a*) $\nu_0 = 0.3$, (*b*) $\nu_0 = 0.4$. For both figures, the coefficient of restitution has been chosen as $e = 0.8$.

A more adequate and rigorous measure for stability is the norm of the matrix exponential $\|\exp(t\boldsymbol{A})\|$ which describes the largest possible amplification of initial unit norm disturbances at a given time,

$$G(t) \equiv \sup_{\boldsymbol{q}_0 \neq 0} \frac{\|\boldsymbol{q}\|}{\|\boldsymbol{q}_0\|} = \sup_{\boldsymbol{q}_0 \neq 0} \frac{\|\exp(t\boldsymbol{A})\boldsymbol{q}_0\|}{\|\boldsymbol{q}_0\|} = \|\exp(t\boldsymbol{A})\|.$$

For the sake of simplicity, we will consider growth in the 2-norm (Euclidean norm),

although a physically more relevant weighted norm can be introduced. The square for the 2-norm for vectors is given as the sum of squares of the individual vector components. The 2-norm for matrices is deduced from the vector norm in the standard way and is most easily computed with the help of the singular value decomposition.

We will first focus our attention on the linear stability in the asymptotic limit of large time which is accurately described by the spectrum. This can be seen by bounding the norm of the matrix exponential in the following way.

$$\exp(\sigma t) \leqslant \|\exp(t\boldsymbol{A})\| = \|\boldsymbol{S}\exp(t\Lambda)\boldsymbol{S}^{-1}\| \leqslant \|\boldsymbol{S}^{-1}\|\,\|\boldsymbol{S}\|\exp(\sigma t),$$

where σ stands for the real part of the least stable eigenvalue. For normal matrices, $\|\boldsymbol{S}^{-1}\|\,\|\boldsymbol{S}\| = 1$ and the lower and upper bound on the matrix exponential norm coincide. Therefore, the behaviour of $\|\exp(t\boldsymbol{A})\|$ for normal $\boldsymbol{A}$ is governed by the real part σ of the least stable eigenvalue for all times. If $\|\boldsymbol{S}^{-1}\|\,\|\boldsymbol{S}\| \gg 1$, i.e. in the case of a non-normal matrix, only the asymptotic behaviour for large times is described by the least stable eigenvalue. Therefore, investigating the spectrum of a non-normal matrix is equivalent to analysing the $t \to \infty$ behaviour of solutions to the associated initial-value problem.

In the next paragraph we will investigate the long term behaviour of our governing equations which have been found to yield a matrix $\boldsymbol{A}$ of non-normal type.

In figure 3 we plot the growth rate (i.e. the real part of the least stable eigenvalue) as a function of the normal wavenumber k_y.

It is interesting to note that for low positive as well as negative normal wavenumbers the curve for the growth rate shows a cusp. This cusp stems from a switching of eigenvalues of the stability matrix $\boldsymbol{A}$ and is associated with a pronounced change in the structure of the least stable eigenmode. To illustrate this further, we plotted the location of the four eigenvalues of system (1) in the complex plane as the normal wavenumber was varied (figure 4*a*). For negative k_y (denoted by *A* in figure 4*a*) the eigenvalue of branch III constitutes the least stable mode. By increasing the normal wavenumber, the eigenvalues of branch I and II will move towards the unstable half-plane taking over the role of the least stable mode (*B*). By further increasing k_y the eigenvalues of branch I and II tend towards higher damping rates (*C* and *D*) and the least stable eigenvalue is associated with branch III. Regarding the least stable mode, the eigenvalue of branch IV does not come into play for this particular choice of parameters. This switching of the eigenvalues results in the cusps in figure 3. Associated with that exchange is also a discontinuous change in the structure of the dominant eigenvector. This is displayed in figure 4(*b*) where the modulus of each eigenvector component has been plotted versus the normal wavenumber k_y for small and positive values of k_y. Besides the jump at the crossing wavenumber $(k_y)_c \approx 0.043$ we also observe the dominance of velocity components in the structure of the least stable eigenvectors.

In figure 5 we computed the asymptotic growth rate for infinitesimal disturbances in the (k_x, k_y)-plane where the linearly unstable region has been shaded. For wavenumbers of physical interest, we observe an extended region of linear instability in the positive k_y-plane and the maximum growth rate is associated with perturbations of the type shown in figure 2(*a*) that form an angle slightly greater than 45° with respect to the streamlines. Only for larger values of k_x and small to moderate normal wavenumbers, is linear stability for $t \to \infty$ encountered although there is a small lobe of instability for perturbation wave vectors approximately perpendicular to the least stable ones in the upper plane. This lobe corresponds to perturbations depicted in figure 2(*b*).

It should be stressed again that the eigenvalue-based stability results are only valid

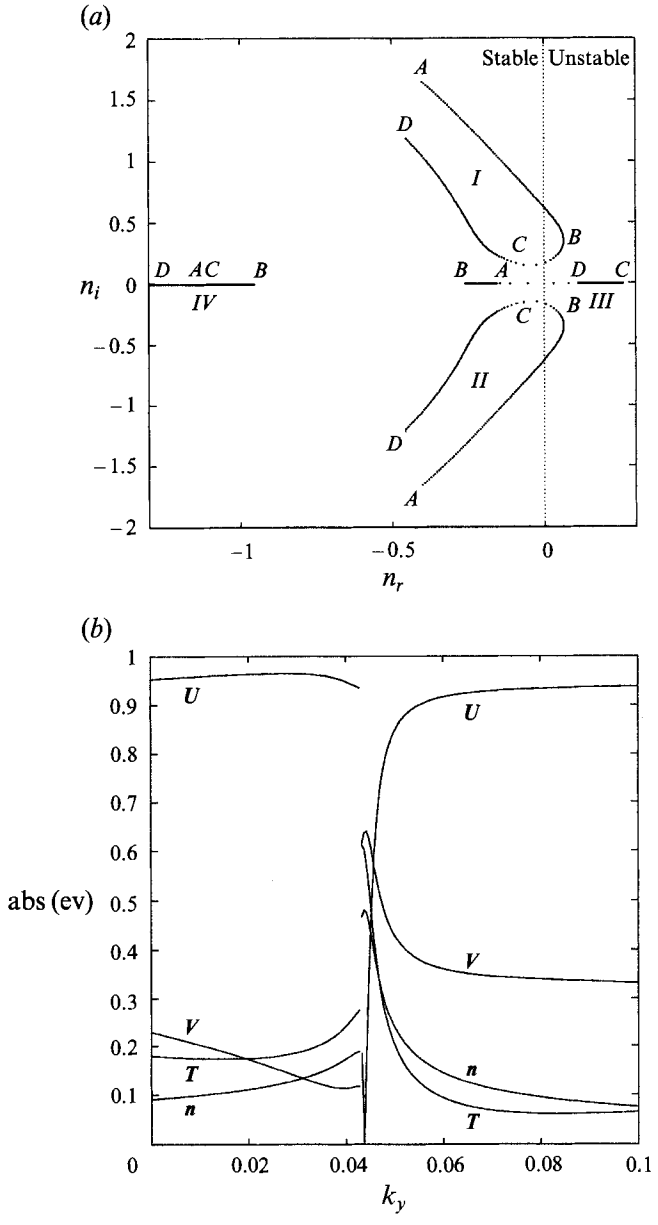

FIGURE 4. Eigenvalue trace and eigenvector structure. In (*a*) the four eigenvalues have been traced in the complex plane as the normal wavenumber k_y has been increased from $k_y = -0.4$ (marked with the letter *A*) to $k_y = 0.4$ (marked with the letter *D*). In (*b*) the absolute value of each eigenvector component associated with the least stable eigenvalue is displayed as a function of k_y. Owing to the eigenvalue switching, a discontinuity is observed at a normal wavenumber of $k_y \approx 0.043$. For both plots a streamwise wavenumber of $k_x = 0.1$, a mean solid fraction of $\nu_0 = 0.3$ and a coefficient of restitution of $e = 0.8$ have been used.

for the asymptotic limit of large time, but do not allow any conclusions about the overall stability of the flow.

We now will focus on the norm of the matrix exponential that will give more insight into the short time stability character of the flow. To this end, we plot the norm of the matrix exponential as a function of time. As can be seen in figure 6, there is a

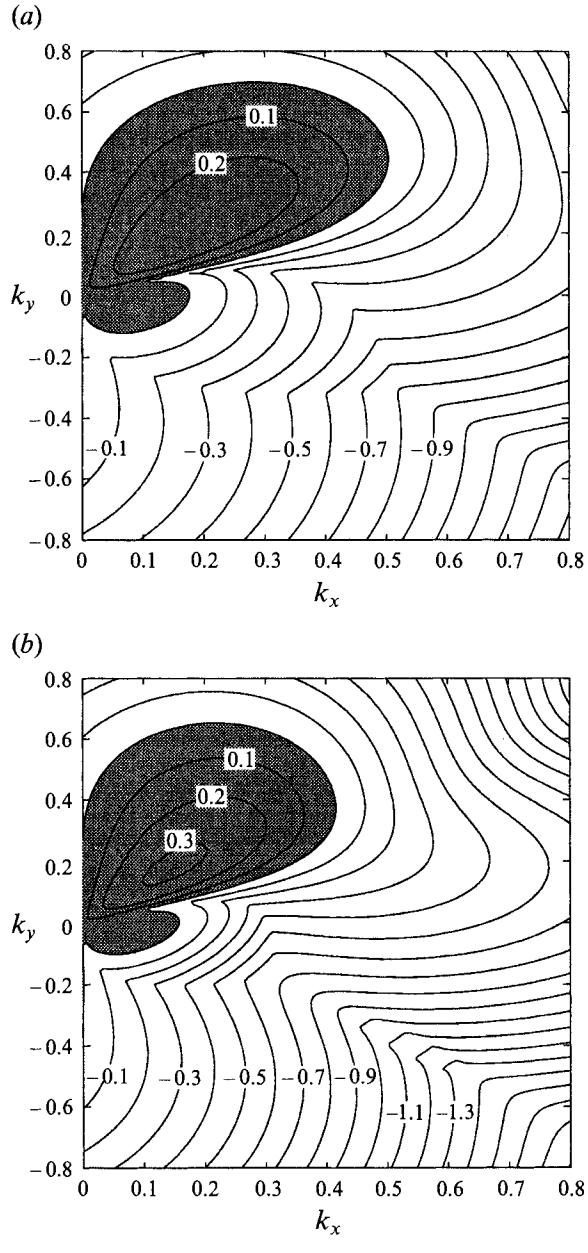

FIGURE 5. Contours of the real part of the least stable eigenvalue. (*a*) for a solid fraction of $\nu_0 = 0.3$; (*b*) for a solid fraction of $\nu_0 = 0.4$. In both cases the coefficient of restitution is $e = 0.8$. The shaded region represents unstable (k_x, k_y)-combinations.

pronounced transient growth period even for the asymptotically decaying flow configuration. For the chosen parameter combination an amplification of the initial energy by a factor of 5.9 is possible before the decay predicted by the (damped) spectrum sets in. This transient growth phase is also present for an asymptotically unstable flow and might provide sufficiently large amplitudes at a much shorter timescale than exponential instabilities will do for finite-amplitude effects to set in.

It is worth emphasizing that the curves depicted in figure 6 represent the envelope of

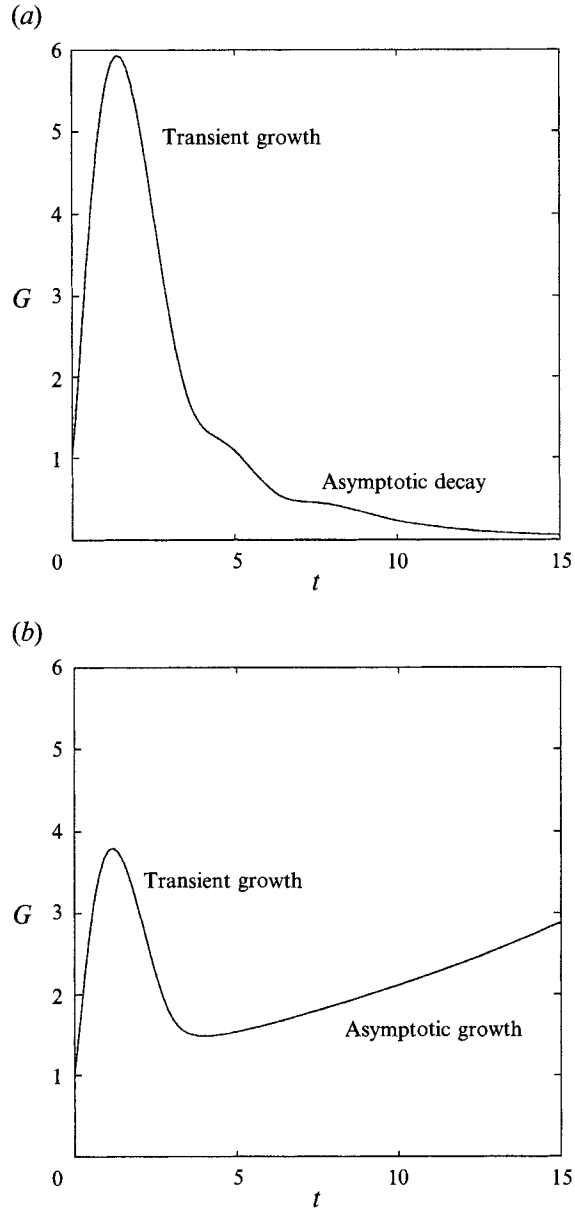

FIGURE 6. Temporal evolution of the norm of the matrix exponential. (*a*) $k_x = 0.4$, $v_0 = 0.3$, $e = 0.8$, $k_y = 0.1$. The asymptotic growth rate has been found to be $n_r = -0.2795$. (*b*) $k_x = 0.4$, $v_0 = 0.3$, $e = 0.8$, $k_y = 0.25$. For this configuration the asymptotic growth rate is $n_r = +0.0625$.

all possible realizations based on initial conditions with the unit 2-norm which is reflected in the definition of $G(t)$ given above. All individual realizations by definition fall below it or at best meet this curve tangentially. Given a tangent point on this envelope, the associated initial condition and subsequent evolution is given as the right and left singular vector of $\exp(t_0 \boldsymbol{A})$, respectively, where t_0 is the time corresponding to the tangent point.

It is important to realize that the transient amplification of the 2-norm of initial perturbations is a non-modal phenomenon which can be seen by computing the

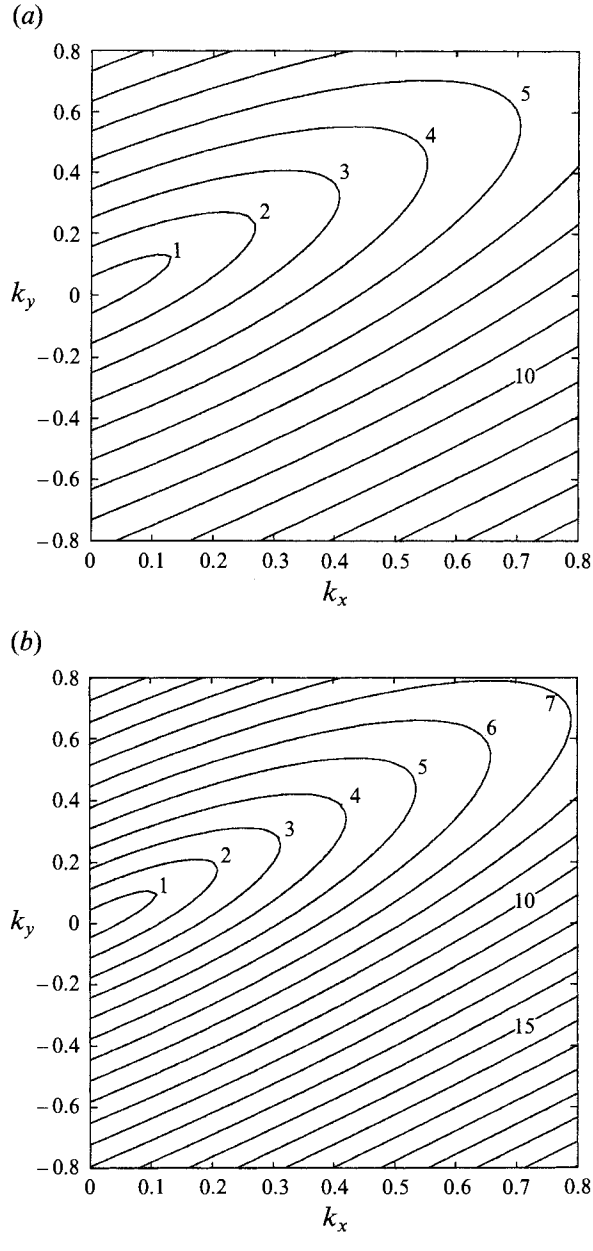

FIGURE 7. Contours of initial transient growth rate in the (k_x, k_y)-plane. (*a*) for a solid fraction of $\nu_0 = 0.3$; (*b*) for a solid fraction of $\nu_0 = 0.4$. In both cases the coefficient of restitution is $e = 0.8$.

	$t_0 = 1.36$	$t_0 = 25$	eigenvector
$\hat{v}$	0.0731	−0.0955	−0.0955
$i\hat{u}$	0.8951	0.0134	0.0218
$i\hat{v}$	−0.2546	−0.9785	−0.9776
$\hat{T}$	−0.3586	−0.1823	−0.1864

TABLE 1. Structure of optimal perturbations tangent to the curve in figure 6(*a*) at selected times.

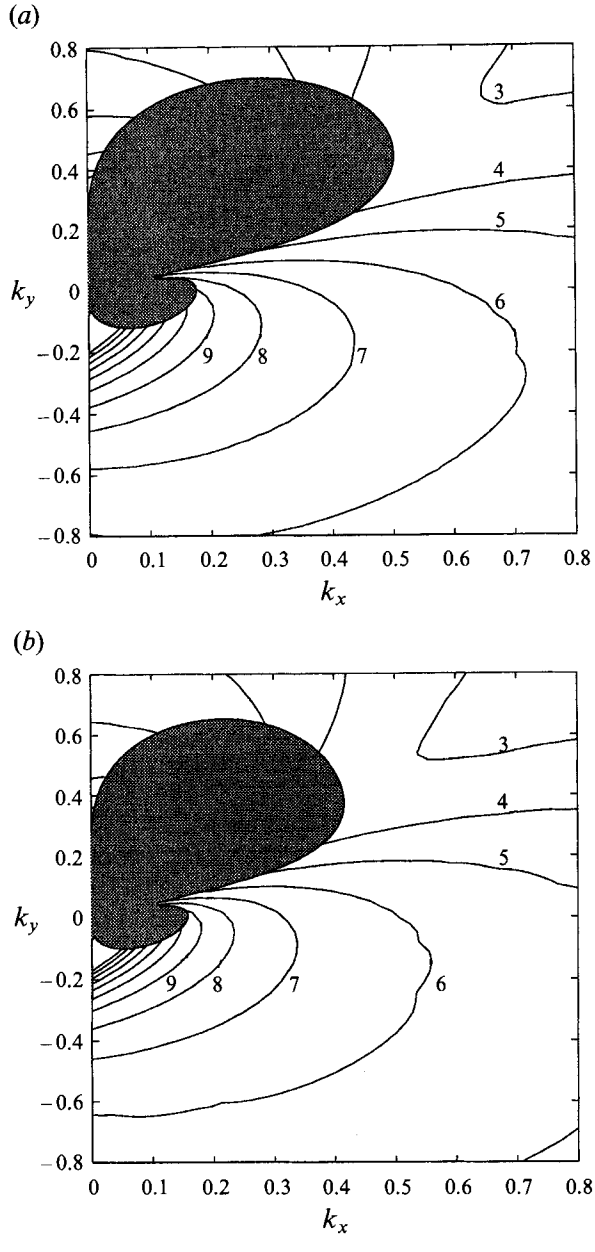

FIGURE 8. Contours of the maximum possible amplification factor in the (k_x, k_y)-plane. The shaded region corresponds to the asymptotically unstable region where infinite amplitudes are possible owing to exponential growth.. The mean solid fraction has been set to $\nu_0 = 0.3$ for (*a*) and to $\nu_0 = 0.4$ for (*b*), the coefficient of restitution is $e = 0.8$.

components of the disturbances that will constitute the maximum growth curves (figure 6) for selected times. The results, obtained by the singular value decomposition, are listed in table 1.

The structure of the disturbance that will reach the maximum possible transient amplification at $t = 1.36$ differs considerably from the disturbance at time $t = 25$ which itself is close to the eigenvector associated with the least stable eigenvalue (see last

column of table 1). Whereas the disturbance at $t = 1.36$ consists mostly of a $\hat{u}$-wave, it is a normal velocity mode that will persist in the limit of large time. This shows that the transient effects observed in figure 6 are inherently non-modal.

Figure 7 displays the initial transient growth rate ω defined as

$$\omega = \frac{1}{\|\boldsymbol{q}\|^2}\frac{\mathrm{d}}{\mathrm{d}t}\|\boldsymbol{q}\|^2 \quad \text{at} \quad t = 0,$$

as a function of streamwise and normal wavenumber. Considerable growth rates are observed throughout the (k_x, k_y)-plane and among the perturbations with fixed wave vector modulus, disturbances with a 45° structure will experience the least initial growth. This initial behaviour markedly differs from the asymptotic result in figure 5 which shows the greatest growth rates just off the 45° line. Furthermore, this result appears to be independent of the mean solid fraction.

Finally, we probe the maximum possible amplification,

$$G_{max} = \sup_{t \geqslant 0} G(t),$$

as a function of the two wavenumbers. Again, the shaded region is the domain of asymptotic instability where infinite amplifications can be achieved owing to an exponential process. Outside this region transient growth is possible and the maximum amplification is given by the corresponding contour levels in figure 8.

3.2. *Turning wave vector case* $\boldsymbol{A}(t) = \boldsymbol{A}_0 + \boldsymbol{A}_1 t + \boldsymbol{A}_2 t^2$

A similar analysis than the one presented in the previous section is developed to allow us to capture transient effects for the variable coefficient case. However, owing to the time dependence of $\boldsymbol{A}$, the equivalent analysis is more involved and makes use of the theory of differential equations for linear operators. For the present case of granular shear flow stability, we are limited to a finite-dimensional linear operator and in what follows we will restrict ourselves to the 4×4 matrix case, although the theory presented is valid for a wider class of linear operators.

It can be shown (e.g. Bellman 1960) that any solution of

$$\frac{\mathrm{d}}{\mathrm{d}t}\boldsymbol{q} = \boldsymbol{A}(t)\,\boldsymbol{q}, \quad \boldsymbol{q}(0) = \boldsymbol{q}_0, \quad \boldsymbol{q}_0, \boldsymbol{q} \in \mathscr{C}^4, \quad \boldsymbol{A} \in \mathscr{C}^{4\times 4}$$

can be written as $\boldsymbol{q} = \boldsymbol{X}\boldsymbol{q}_0$ where $\boldsymbol{X}$ is known as the normalized integral matrix or the fundamental matrix and satisfies the matrix differential equation

$$\frac{\mathrm{d}}{\mathrm{d}t}\boldsymbol{X} = \boldsymbol{A}\boldsymbol{X}, \quad \boldsymbol{X}(0) = \boldsymbol{I}, \quad \boldsymbol{X}, \boldsymbol{I} \in \mathscr{C}^{4\times 4}$$

where $\boldsymbol{I}$ denotes the identity matrix.

This matrix differential equation can be solved by the method of successive approximation.

Let $\boldsymbol{X}^{(0)} = \boldsymbol{I}$ and $\boldsymbol{X}^{(i)}(t)$ denote the fundamental matrix after the ith iteration; then the next approximation is given by

$$\boldsymbol{X}^{(i+1)}(t) = \boldsymbol{I} + \int_0^t \boldsymbol{A}(\tau)\,\boldsymbol{X}^{(i)}(\tau)\,\mathrm{d}\tau, \tag{2}$$

where the fact that

$$\boldsymbol{X}^{(i+1)}(0) = \boldsymbol{I}$$

has been used. The integral of the matrices is taken component-wise.

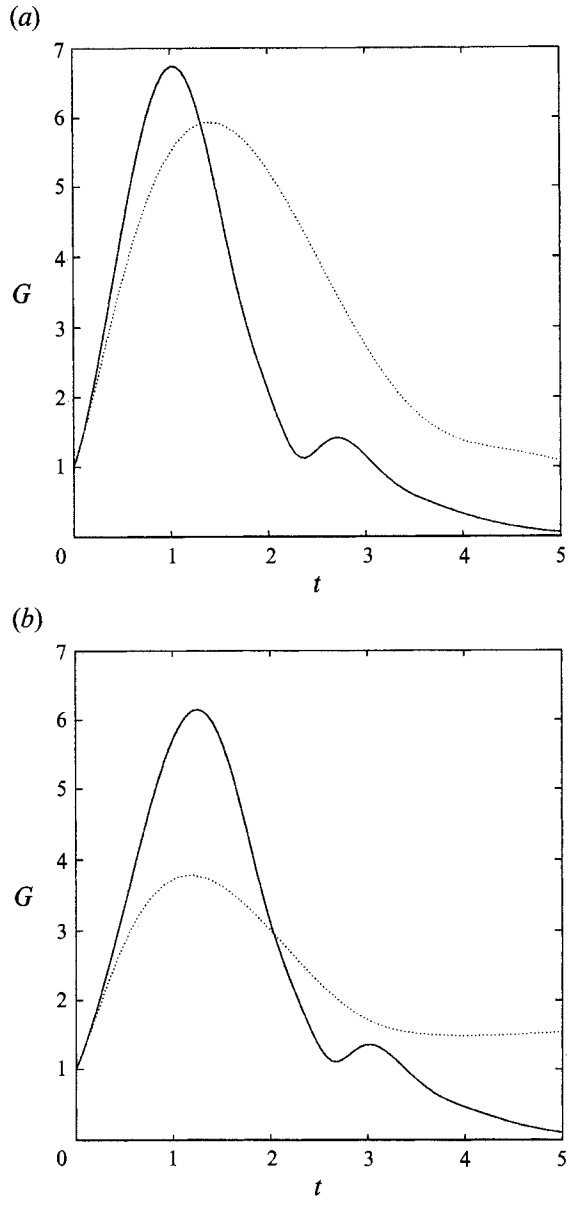

FIGURE 9. Temporal evolution of the norm of the fundamental matrix for the variable coefficient case (i.e. shear-induced wave vector turning). (*a*) $k_x(0) = 0.4$, $\nu_0 = 0.3$, $e = 0.8$, $k_y(0) = 0.1$. (*b*) $k_x(0) = 0.4$, $\nu_0 = 0.3$, $e = 0.8$, $k_y(0) = 0.25$. The dotted line in both figures is the temporal evolution of the matrix exponential norm for the constant coefficient case with otherwise identical parameter setting and is given for comparison.

The approximations $\boldsymbol{X}^{(i)}(t)$ can be written explicitly in form of nested integrals of the coefficient matrix $\boldsymbol{A}(t)$ as

$$\boldsymbol{X}^{(0)} = \boldsymbol{I},$$

$$\boldsymbol{X}^{(i)} = \boldsymbol{I} + \underbrace{\int_0^t \boldsymbol{A}(\tau) \int_0^\tau \boldsymbol{A}(\sigma) \ldots \mathrm{d}\sigma \, \mathrm{d}\tau}_{i \text{ times}}.$$

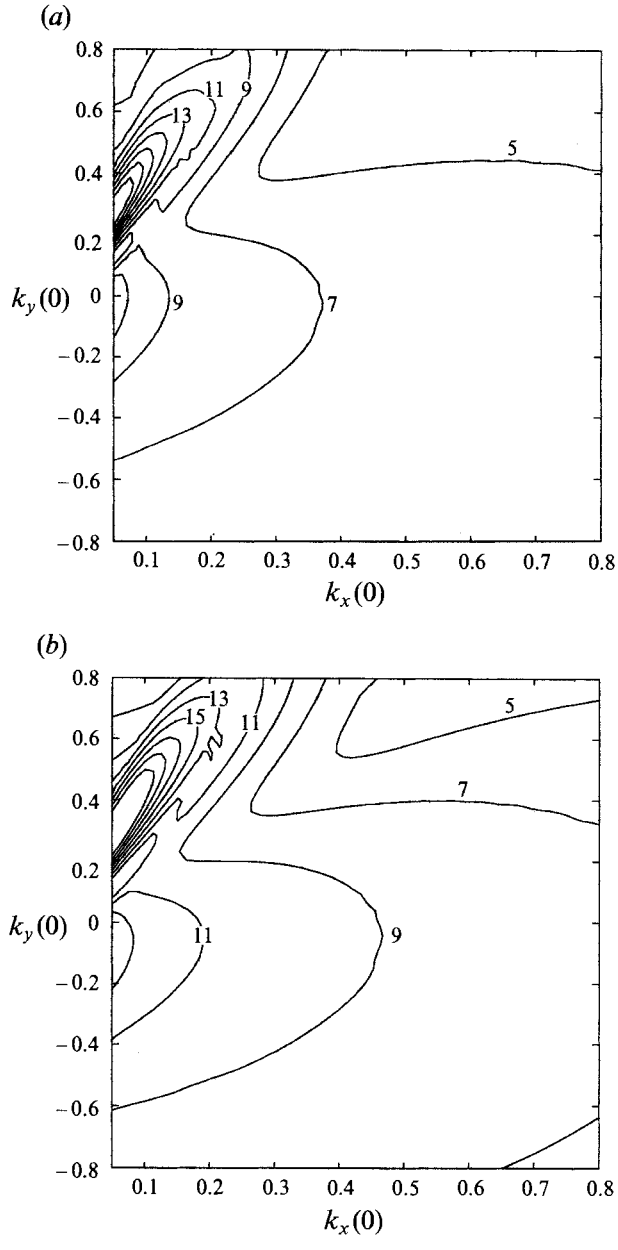

FIGURE 10. Contours of the maximum possible amplification factor in the (k_x, k_y)-plane for the variable coefficient case (i.e. shear-induced wave vector turning). The mean solid fraction has been set to $\nu_0 = 0.3$ for (*a*) and $\nu_0 = 0.2$ for (*b*), the coefficient of restitution is $e = 0.8$.

The fundamental matrix $\boldsymbol{X}(t)$ is then given as

$$\boldsymbol{X}(t) = \lim_{i \to \infty} \boldsymbol{X}^{(i)}(t).$$

Other solutions to the matrix differential equation for $\boldsymbol{X}(t)$ are known, one of them leading to an exponential form similar to the constant coefficient case (Magnus 1954). The solution by multiplicative integrals is also an alternative to the recurrence technique given above. For further details the reader is referred to Gantmacher (1989).

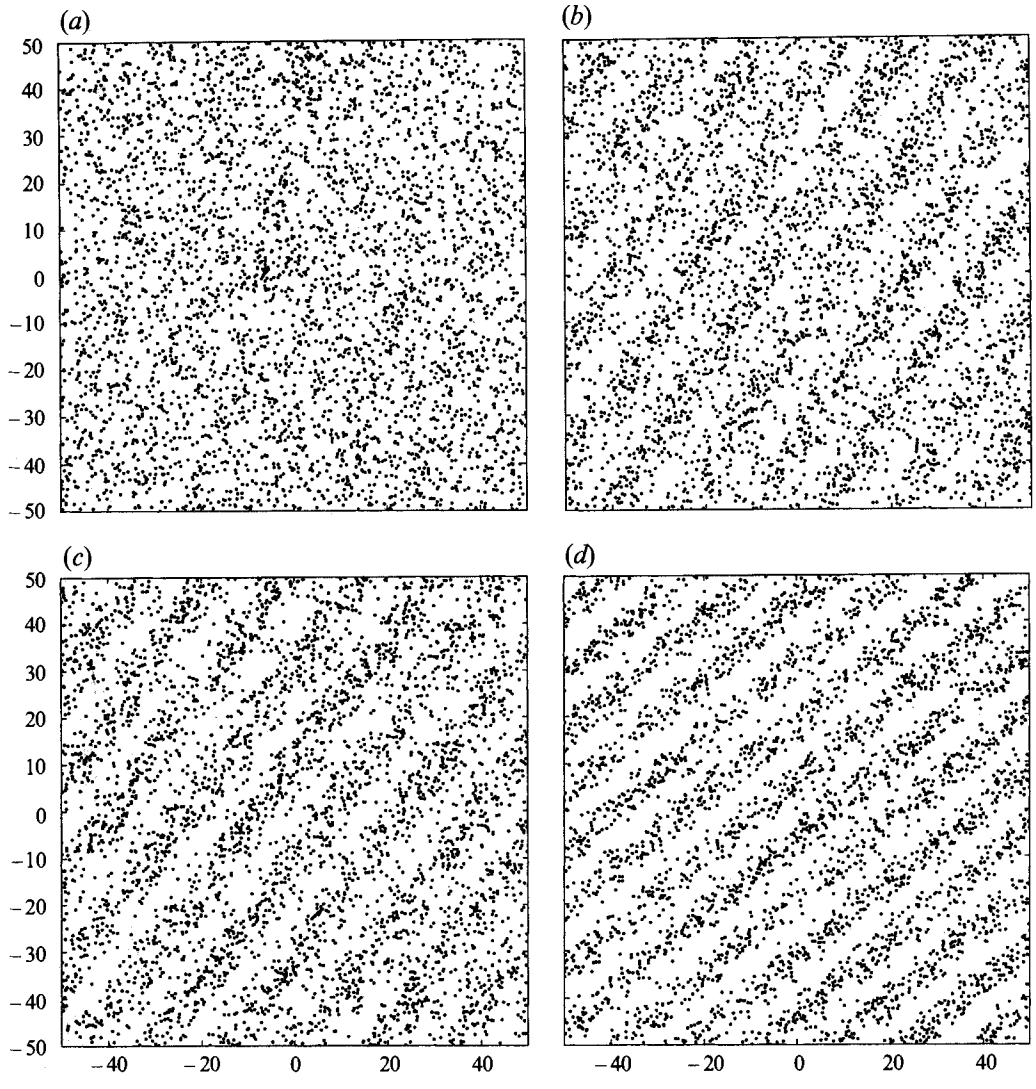

FIGURE 11(*a–d*). For caption see facing page.

It should be noted that for the case of a constant coefficient matrix $\boldsymbol{A}$, the algorithm above will result in the matrix exponential $\boldsymbol{X}(t) = \exp(t\boldsymbol{A})$.

For numerical purposes, the evaluation of the integrals by Romberg's method has been found to be sufficient. The number of iterations appeared to be dependent on the governing parameters and the convergence of the results required particular care.

The recurrence relation (2) is absolutely and uniformly convergent in the interval $[0, T]$, and an outline of the proof is given in Gantmacher (1989).

Applying the above to our problem, we are now able to cast the stability equations for turning wave vectors into an analogous form as for the constant wave vector case, i.e.

$$G(t) \equiv \sup_{\boldsymbol{q}_0 \neq 0} \frac{\|\boldsymbol{q}\|}{\|\boldsymbol{q}_0\|} = \sup_{\boldsymbol{q}_0 \neq 0} \frac{\|\boldsymbol{X}(t)\,\boldsymbol{q}_0\|}{\|\boldsymbol{q}_0\|} = \|\boldsymbol{X}(t)\|.$$

In this case, the 2-norm of the fundamental matrix is the proper measure to decide on stability or instability of the fluid system.

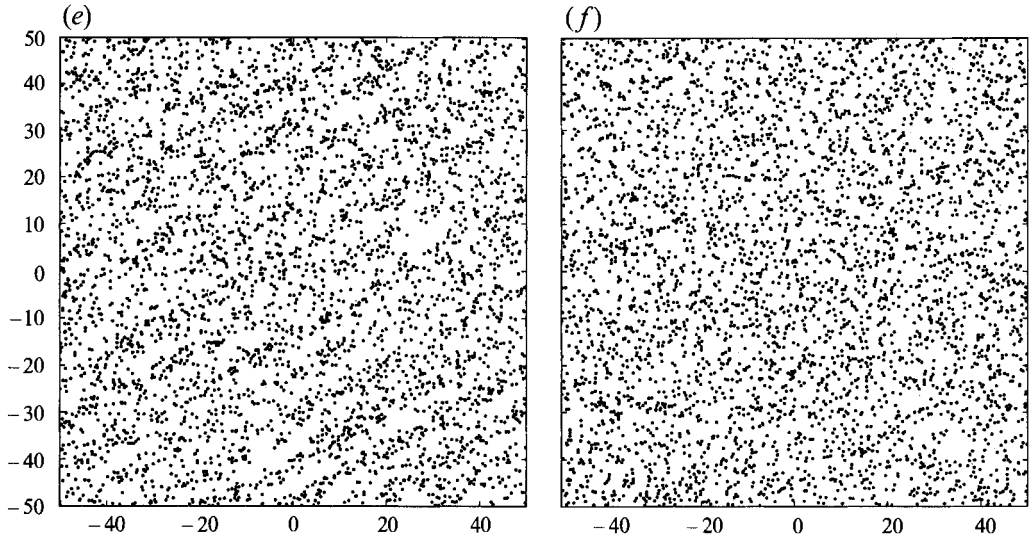

FIGURE 11. Visualization of the solid fraction perturbation for (*a*) $t = 1$, (*b*) $t = 1.4$, (*c*) $t = 1.5$, (*d*) $t = 2$, (*e*) $t = 2.5$ and (*f*) $t = 3$. The chosen parameters are $k_x(0) = 0.4$, $k_y(0) = 0.1$, $\nu_0 = 0.3$, $e = 0.8$. A decrease in the density of points in the scatter plot reflects a decrease in solid fraction while an increase in the density reflects an increase in the solid fraction. The initial perturbation is in the normal velocity $\hat{v}$ alone, hence the homogeneous appearance of the concentration distribution at early times.

In figure 9 $\|\boldsymbol{X}(t)\|$ is plotted as a function of time and as in the case of constant wavenumbers, transient growth is observed. Another interesting feature arises from the asymptotic analysis. It shows that for large times and $k_x(0) \neq 0$, the different components of the disturbance vector $(\hat{v}\,\hat{u}\,\hat{v}\,\hat{T})^T$ decouple and behave like

$$\hat{u} \sim \exp(-C_u t^3),$$
$$\hat{v} \sim \exp(-C_v t^3),$$
$$\hat{T} \sim \exp(-C_T t^3),$$

where

$$C_u = \frac{1}{6\nu_0} F_2|_o\, k_x^2(0) > 0,$$

$$C_v = \frac{1}{3\nu_0}(\alpha_0 + \tfrac{2}{3}F_2|_o)\, k_x^2(0) > 0,$$

$$C_T = \frac{2}{9\nu_0} K_0\, k_x^2(0) > 0,$$

thus showing absolute stability of $\hat{u}, \hat{v}$ and $\hat{T}$. The behaviour of $\hat{v}$ for large time is characterized by asymptotic decay, as can easily be seen from the governing equations given in §2.

Therefore, in the case of shear induced wave vector turning the disturbances show no asymptotic instability for all physically meaningful parameter combinations, and instabilities for this case are only possible through the transient mechanism.

Transient effects might trigger high-amplitude phenomena (i.e. nonlinearities) and the asymptotic (stable) limit for large times may never be observed in an experimental setting.

The dotted line in the plots represents the solution of the constant wavenumber case

based on the same parameters. It has been added to show the different behaviour of the two systems. The initial growth rate for the variable coefficient case coincides for obvious reasons with the one for the constant matrix $\boldsymbol{A}$ (figure 7). This is also reflected in the identical initial slope of the solid and dotted line in figure 9 for $t = 0$. The turning wave case appears to result in larger amplification of the 2-norm than the equivalent non-turning case and the time of occurrence of the transient peak does not coincide with its equivalent in the non-turning case.

The dependence of the maximum amplification for a range of streamwise and normal wavenumbers is displayed in figure 10 for a combination of selected parameter values. This figure shows that the largest linear growth occurs for very small values of $k_x(0)$ and at about $k_y(0) \approx 0.3$. Such perturbations result in the largest subsequent amplification of the 2-norm of the perturbation vector, and as the wavenumber vector turns during growth, the appearance of the instability strongly depends on the time at which it reaches a maximum. Since we only consider the 2-norm, no conclusions can be drawn on the nature of the perturbation or which flow variable is most amplified.

To illustrate the transient growth and asymptotic decay process in the case of a wavelike perturbation that is allowed to turn with the imposed constant shear, we computed the evolution of the perturbation in solid fraction for selected times starting with an initial disturbance that consists of a pure normal velocity ($\hat{v}$) perturbation of unit 2-norm. The initial-value problem was solved numerically using a fourth-order Runge–Kutta scheme. The minimum solid fraction encountered within the time interval of integration was subtracted from the calculated solid fraction and the result was normalized by its maximum peak to peak value. This was then used as a probability density function to visualize the formation and decay of coherent patterns. The results are displayed in figure 11. At time $t = 0$ no initial perturbation in solid fraction is imposed. As time evolves, a distinct structure appears that subsequently turns 'into the shear'. At later times, this structure experiences considerable stretching which ultimately results in a completely homogeneous mixture. Although the analysis predicts asymptotic decay of perturbations for all physical parameter combinations, it is conceivable that during the process displayed in figure 11 finite-amplitude effects may be triggered that will yield permanent microstructures as observed in the simulations of Hopkins & Louge (1991). This particular realization is for a prescribed wavenumber initial condition. Owing to the discrete nature of real systems, their transient behaviour is governed by the evolution of broadband noise as an initial condition. This can be simulated by the superposition of the full range of physical wavenumbers in the (k_x, k_y)-plane.

4. Summary and conclusions

This study builds upon the current understanding of linear stability of granular shear flows, using the continuum governing equations first presented by Lun *et al.* (1984). In the context of inertially dominated particulate flows, Savage (1992) gave a presentation of the asymptotic stability of these systems which was also used by Babić (1992, 1993). Here, we discuss the transient stability of stationary harmonic perturbations as well as harmonic perturbations that turn with the imposed shear, and revisit asymptotic stability with new findings.

4.1. *Asymptotic stability*

The constant wavenumber case revealed two modes of asymptotic instability, that favour the most rapid growth of perturbations with approximately perpendicular wavenumber vectors. Savage (1992) fully documented the stability of structures in the

upper right-hand quadrant of the (k_x, k_y)-plane, but neglected to document the nature of the lower right-hand quadrant. The regions of instability appear as lobes in the (k_x, k_y)-plane. These are separated by a discontinuous slope in the growth constant of the least stable mode. In figure 5, this is evident from the cusp in the contour map of the growth constant and reflects a switch in the eigenvector of the most unstable mode. With a broadband initial perturbation, the combination of the maxima in growth rate of the two lobes of instability can be expected to asymptotically yield the dominant structures, within the limitations of linear theory. These structures are made up of two sinusoids of near perpendicular wavenumber vectors (for the cases studied, the angle between the wavenumber vectors was 89.7°). Figure 4 shows that the eigenvectors associated with the two modes both have non-zero components of all four flow variables. Therefore, both lobes will influence the particle distribution, and the two modes will constructively and destructively interfere with one another to create geometrically arranged visible ellipsoidal 'structures' nested in near rectangular parallelograms. The aspect ratio of these ellipses is approximately the ratio of the magnitude of the wavenumber vectors associated with the lobe maxima, and their length is the reciprocal of the magnitude of the lower lobe wavenumber vector. The orientation of the major axis is derived from the orientation of the upper lobe wavenumber vector, as had been shown by Savage (1992), and it 'opposes' the shearing motion. Babić (1992, 1993) identified the two lobes of asymptotic instability in the (k_x, k_y)-plane, but did not associate them with the formation of coherent structures.

For example, at a solid fraction of $\nu_0 = 0.4$, and $e = 0.8$, the aspect ratio of the linearly unstable structures is approximately 3.8. In general, the angle of the major axis of these structures relative to the streamline is not 45° as may have been suggested by others, for this example it is 50.7°, and they are approximately 26 particle diameters long.

The turning wavenumber case is found to be asymptotically stable for all wavenumbers and all orientations of the initial perturbation.

4.2. *Transient stability*

One of the main points made in this paper is the distinction between asymptotic and transient instability for non-normal systems. Whereas the former is governed by the spectrum of the linear evolution operator, the latter requires more sophisticated tools to capture the short-time characteristics of the flow. A correct measure of the (in)stability is given by the norm of the solution operator.

For both cases of constant and time-varying wavenumber vector, a period of significant transient growth has been observed followed by behaviour that is dictated by the spectrum of the linearized operator. The maximum possible amplification of the 2-norm of the initial condition is larger for wavelike disturbances that exhibit time-dependent alignment with the imposed main shear field than for perturbations that do not change their spatial structures as time progresses. The perturbations that lead to the greatest amplification were found to be nearly aligned with the flow. Owing to the asymptotic stability of the turning wave vector scenario, large growth and development of finite-amplitude effects can only be achieved with the help of the transient instability mechanism shown in this presentation.

Owing to the discrete nature of most granular flows, which can often be described as occupying a volume that is not significantly larger than the volume of an individual particle, thereby violating the requirements of a continuum, broadband noise in all flow variables is inherently present. This will continually feed the transient growth process illustrated in figure 11, and will result in persistent visible microstructure whose

major axis is 'aligned' with the shear (south-west to north-east in the figure), as was observed by Hopkins & Louge (1991). As the transient growth process is found to be stronger in the turning wave case, this mechanism is believed to dominate over the asymptotic fixed wavenumber instability for a range of conditions; specifically those where the fixed wavenumber asymptotic growth is sufficiently small. Indeed, the asymptotic microstructure predicted by Savage (1992) and Babić (1992, 1993) 'opposes' the shear in contradiction with numerical observations and the continual transient growth mechanism owing to inherent broadband noise.

Finally, while this mechanism may be the dominant source of coherent pattern formation, it may also provide a mechanism for triggering finite-amplitude effects.

The authors gratefully acknowledge the generous support of Intevep, the Research and Technological Center of Petroleós de Venezuela.

REFERENCES

ANDERSON, T. B. & JACKSON, R. 1968 Fluid mechanical description of fluidized beds. *I&EC Fundamentals*, pp. 12–21.

BABIĆ, M. 1992 Particle clustering: an instability of rapid granular flows. In *Advances in Micromechanics of Granular Materials* (ed. H. H. Shen, M. Satake, M. Mehrabadi, C. S. Chang & C. S. Campbell). Elsevier.

BABIĆ, M. 1993 On the stability of rapid granular flows. *J. Fluid Mech.* **254**, 127–150.

BAGNOLD, R. A. 1954 Experiments on a gravity free dispersion of large solid spheres in a Newtonian fluid. *Proc. R. Soc. Lond.* **225**, 49–63.

BARNES, H. A. 1989 Shear-thickening in suspension of non-aggregating solid particles dispersed in Newtonian liquids. *J. Rheol.* **33**, 329–366.

BATCHELOR, G. K. 1988 A new theory of the instability of a uniform fluidized bed. *J. Fluid Mech.* **193**, 75–110.

BELLMAN, R. 1960 *Introduction to Matrix Analysis*. McGraw-Hill.

BUTLER, K. M. & FARRELL, B. F. 1992 Three-dimensional optimal perturbations in viscous shear flow. *Phys. Fluids* A **4**, 1637–1650.

CAMPBELL, C. S. 1990 Rapid granular flows. *Ann. Rev. Fluid Mech.* **22**, 57–92.

CAMPBELL, C. S. & BRENNEN, C. E. 1985 Computer simulations of granular shear flows. *J. Fluid Mech.* **151**, 167–188.

FARRELL, B. F. & IOANNOU, P. J. 1993 Optimal excitation of three-dimensional perturbations in viscous constant shear flow. *Phys. Fluids* A **5**, 1390–1400.

FOSCOLO, P. U. & GIBILARO, L. G. 1987 Fluid dynamic stability of fluidized suspensions: the particle bed model. *Chem. Engng. Sci.* **42**, 1489–1500.

GANTMACHER, F. R. 1989 *Matrix Theory*. Chelsea.

HAFF, P. K. 1983 Grain flow as a fluid-mechanical phenomenon. *J. Fluid Mech.* **134**, 401–430.

HILL, C. D. & BEDFORD, A. 1979 Stability of the equations for particulate sediment. *Phys. Fluids* **22**, 1252–1254.

HOPKINS, M. A. & LOUGE, M. Y. 1991 Inelastic microstructure in rapid granular flows of smooth disks. *Phys. Fluids* A **3**, 47–57.

HOMSY, G. M., EL-KAISSY, M. M. & DIDWANIA, A. 1980 Instability waves and the origin of bubbles in fluidized beds – II, Comparison with theory. *Intl J. Multiphase Flow* **6**, 305–318.

JACKSON, R. 1985 Hydrodynamic stability of fluid-particle systems. In *Fluidization* (ed. J. F. Davidson, R. Clift & D. Harrison), Chap. 2. Academic Press.

JENKINS, J. T. & SAVAGE, S. B. 1983 A theory for the rapid flow of identical, smooth, nearly elastic particles. *J. Fluid Mech.* **130**, 187–202.

LUN, C. K., SAVAGE, S. B., JEFFREY, D. J. & CHEPURNIY, N. 1984 Kinetic theories for granular flow: inelastic particles in Couette flow and slightly inelastic particles in a general flow field. *J. Fluid Mech.* **140**, 223–256.

McNAMARA, S. 1993 Hydrodynamic modes of a uniform granular medium. *Phys. Fluids* A **5**, 3056–3070.

MAGNUS, W. 1954 On the exponential solution of differential equations for a linear operator. *Commun. Pure Appl. Maths* **7**, 649–673.

MELLO, T. M., DIAMOND, P. H. & LEVINE, H. 1991 Hydrodynamic modes of a granular shear flow. *Phys. Fluids* A **3**, 2067–2075.

PHILLIPS, O. M. 1969 Shear flow turbulence. *Ann. Rev. Fluid Mech.* **1**, 245–264.

PROSPERETTI, A. & JONES, A. V. 1987 The linear stability of general two-phase flow models – II *Intl J. Multiphase Flow* **13**, 161–171.

REDDY, S. C. & HENNINGSON, D. S. 1993 Energy growth in viscous channel flows. *J. Fluid Mech.* **252**, 209–238.

REDDY, S. C., SCHMID, P. J. & HENNINGSON, D. S. 1993 Pseudospectra of the Orr–Sommerfeld operator. *SIAM J. Appl. Maths.* **53**, 15–45.

SAVAGE, S. B. 1992 Instability of 'unbounded' uniform granular shear flow. *J. Fluid Mech.* **241**, 109–123.

TREFETHEN, L. N., TREFETHEN, A. E., REDDY, S. C. & DRISCOLL, T. 1993 Hydrodynamic stability without eigenvalues. *Science* **261**, 578–584.

WALTON, O. R., KIM, H. & ROSATO, A. 1991 Micro-structure and stress differences in shearing flows. In *Mechanics and Computing in 1990's and Beyond* (ed. H. Adeli & R. L. Sierakowski), vol. 2, pp. 1249–1253. ASCE.